Optik - International Journal for Light and Electron Optics 218 (2020) 165106

Contents lists available at ScienceDirect

Optik

journal homepage: www.elsevier.com/locate/ijleo

Influence of calcination temperature on the photoluminescence spectral response of Sm-doped YAG nanocrystals as red-emitting phosphor

Hanan Ali, Alaa E. Giba*, Mohamed Atta Khedr

National Institute of Laser Enhanced Sciences, Cairo University, 12613, Giza, Egypt

ARTICLE INFO

Keywords:
YAG Nanocrystals
Samarium emission
Calcination temperature

ABSTRACT

This work reports on the synthesis of samarium-doped yttrium aluminum garnet nanocrystals via co-precipitation method. The effect of calcination temperature on the formation of the crystalline phase of the prepared powder has been studied. The as-prepared powder was transformed from the amorphous to crystalline phase at calcination temperature around 900 °C, and the crystallite size enhanced at higher calcination temperature, 1000 °C. The crystallization temperature of the prepared YAG powder was measured using differential thermal analysis technique and confirmed by X-ray diffraction. Moreover, the correlation between this phase transformation and the photoluminescence (PL) spectral response of Sm ions has been established. The effect of the crystal field of the environment around Sm ions on its PL spectral response is also discussed. Furthermore, the excitation levels of Sm^{3+}-doped YAG nanocrystals have been measured. These findings attempt to highlight on the role of PL in probing the local environment of such phosphor.

1. Introduction

Phosphors based ceramics have shown great interest due to its significant marketing in lighting and displays applications. For instance, the market of lighting is shifted from incandescent to fluorescent to solid state. This rapid development makes the synthesis issues are of great interest to meet the application requirements. In order to achieve these requirements, structure characteristics such as, high phase purity, high crystallinity, homogeneous distribution of the activator ion, spherical shape, fine particle size, and narrow size distribution were highly demanded. Two main routes are generally followed in preparation of the precursor powders for ceramic fabrication. First route, called *solid-state reaction* process, in which the powders can be prepared using solids, such as oxides, hydroxides, and carbonates, as starting materials [1]. On the other side, the second route is concerned with *wet-chemical methods* such as chemical precipitation or co-precipitation [2,3], sol–gel [4], gel combustion [5] and hydrothermal synthesis [6]. Beside the *solid-state reaction* process, co-precipitation route exhibits great interest and remains among the most widely used synthesis technique for commercial phosphors [1]. However, synthesis of RE-doped YAG nanopowders, with desired sinterability and microstructures, is still a challenge from the chemical point of view. It is found that the structural and functional properties of the nanopowders are strongly affected by many factors; such as solvents, precipitants, reaction temperature, pH values, aging time, and calcination temperature, which need to be carefully controlled [3,7–9]. YAG nanopowders can be synthesized by co-precipitation techniques via two routes; normal strike and reverse strike. The Advantage of reverse strike route, over normal one, is established owing to allowing all the cations to be precipitated at the same time. Hence, better homogeneity of the precipitate can be obtained. For instance, Apte et al.

* Corresponding author.
E-mail address: alaadin85@niles.edu.eg (A.E. Giba).

https://doi.org/10.1016/j.ijleo.2020.165106
Received 30 March 2020; Accepted 5 June 2020

[10] synthesized powders from nitrate salts via normal and reverse strike co-precipitations. The powders prepared via normal strike reveal presence of two phases, Y_2O_3 and YAM, after calcination at 1000 °C. On the contrary, the reverse strike results in pure YAG phase at lower calcination temperature [10]. In the same line, Li et al. also found that YAG samples prepared by normal strike were contaminated by YAM phase even when calcined at 1500 °C. While pure YAG phase was achieved at 1000 °C via reverse strike [11,12]. In addition, Verma et al. concluded, by considering the optical properties of the end product, that reverse strike co-precipitation is a favorable method for synthesizing pure phase of YAG nanopowders, while normal strike is a better option for yttrium gallium garnet (YGG) [13]. This is the reason behind our choice of reverse strike co-precipitation method in the present work. By considering all the chemistry related parameters in the preparation method, calcination temperature exhibits significant influence on the phase purity. Tiecheng Lu et al. [14] showed the effect of calcination temperature of Nd:YAG nanopowders on the transparency of the final ceramic. The authors referred the improvement of the optical properties of the ceramic to the optimization of the calcination temperature which induced better crystalline nano-sized powder. However, to our best of knowledge, the influence of the calcination temperature and the transformation from amorphous to crystalline phase on the PL spectral response of Sm-doped YAG powder has not been reported. Hence, this study presents a correlation between the calcination temperature and the PL spectral and color responses of Sm-doped YAG prepared by reverse strike co-precipitation. Hopefully, it provides some significant missing information in this direction.

2. Experimental section

Samarium doped yttrium aluminum garnet has been prepared via reverse strike co-precipitation method. High purity of nitrite precursors such as; $Y(NO_3)3{\cdot}6H_2O$, $Al(NO_3)_3{\cdot}9H_2O$, and $Sm(NO_3)_3{\cdot}6H_2O$ were used. The precursors were mixed in aqueous solution to appropriate molar ratio to obtain this stoichiometric formula, $Sm_{0.06}Y_{2.94}Al_5O_{12}$. A 0.5 M of ammonium hydrogen carbonate (NH_4HCO_3) was prepared by dissolved in distilled water. The salt solution was added to the precipitant solution to form the precipitation at pH = 7.9. Then it has been aged for 12 h, then filtered and washed with water and ethanol. After drying the precipitation at 80 °C for 24 h, it divided into some parties for calcination in air at different temperatures 800 °C, 900 °C and 1000 °C for 2 h. The phase structure of formed powder was characterized using X-ray diffraction (Philips Analytical X-Ray, 0.154 nm for CuKα). In addition, the average particle size has been determined by scanning electron microscope (SEM). Differential thermal analyzer (DTA) and thermal gravimetric analysis (TGA) were measured to identify the crystallization temperature and the weight loss due to thermal decomposition. Fourier-transform infrared spectroscopy (FTIR) analysis was performed to characterize the chemical bonds. Spectrofluorometer (model; VARIAN CARY 5000) was used for photoluminescence (PL) measurements.

3. Results and discussions

3.1. X-ray diffraction (XRD) and scanning electron microscope (SEM)

X-Ray Diffraction (XRD) is used for testing the phase purity of YAG nanopowders. XRD patterns of as-prepared and calcined powders at (800 °C, 900 °C, and 1000 °C for 2 h), are shown in Fig. 1 (a). No detectable diffraction peaks can be observed from the as-prepared sample. For sample calcined at 800 °C, a small broad band centered at 33.42° degree is observed, which likely points to the onset of crystallization of the YAG phase. In addition, the XRD patterns reveal diffraction peaks of crystalline YAG, at 900 °C and 1000 °C, agree with standard profile of (PDF# 33−0040) and without detection of any secondary phases from the Y_2O_3-Al_2O_3 binary system such as $YAlO_3$ (YAP) or $Y_4Al_2O_9$ (YAM) [15]. Moreover, no other phases due to the incorporation of rare earth ions such as

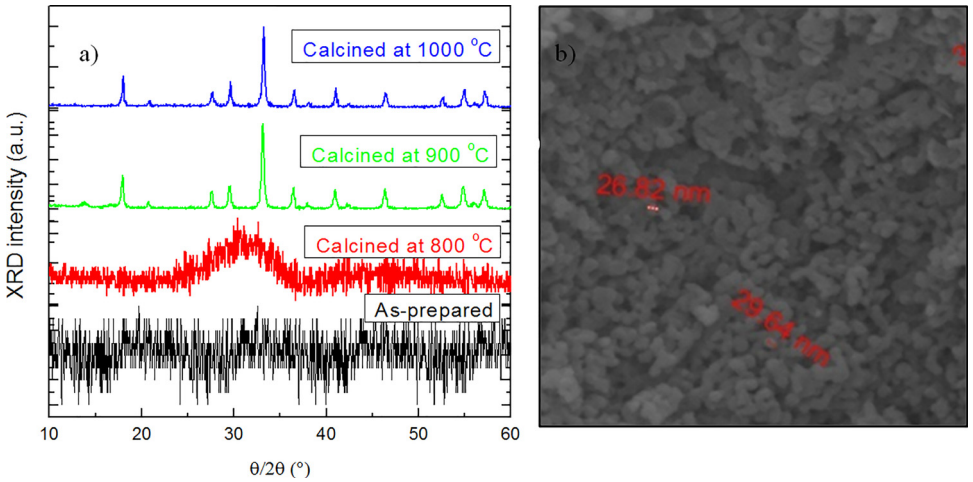

Fig. 1. (a) XRD of $Sm_{0.06}Y_{2.94}Al_5O_{12}$ nanopowders as-prepared and calcined at 800 °C, 900 °C, 1000 °C for 2 h. (b) SEM image of $Sm_{0.06}Y_{2.94}Al_5O_{12}$ nanopowders calcined at 1000 °C.

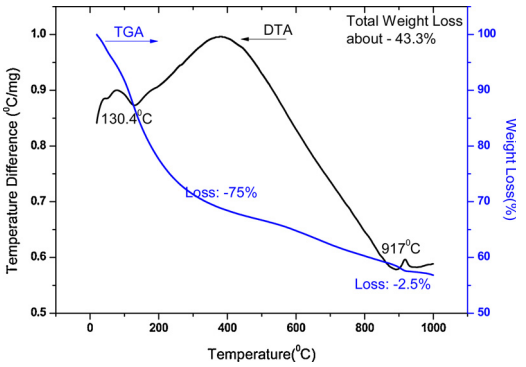

Fig. 2. TGA and DTA curves of $Sm_{0.06}Y_{2.94}Al_5O_{12}$ powder calcined at 1000 °C/2 h.

Sm-oxides are observed. This indicates that pure YAG phase has been realized at low calcined temperatures, 900 °C and 1000 °C, compared to other preparation methods such as the solid-state reaction (SSR) method, where pure YAG phase was obtained at 1500 °C–1600 °C [16]. The formation of pure YAG phase at such low calcination temperatures can be attributed to the shorter diffusion distance between the reactants in co-precipitation method owing to the fine grain size of the precipitated carbonate precursor. This result is in good agreement with the calcination temperatures reported by Li et al. [7] using the reverse-strike method. However Jiang Li's [11] reported different calcination temperatures for obtaining pure YAG phase, in which the pure YAG phase was realized at around 1200 °C. They referred the reason of higher calcination temperature due to the preparation by the normal-strike method. It can be also observed that, elevation of the calcination temperature led to increase in the diffraction peak intensity and a decrease of its full-width at half-maximum (FWHM) due to the improvement of crystallinity and the coarsening of the formed grains. In addition, SEM of $Sm_{0.06}Y_{2.94}Al_5O_{12}$ nanopowders calcined at 1000 °C, Fig. (1 b), shows good dispersity of weak agglomerated particles with estimated particle size around (26 nm–30 nm).

3.2. Thermal analysis

The thermal decomposition and the crystallization temperature of $Sm_{0.06}Y_{2.94}Al_5O_{12}$ were studied by DTA-TGA simultaneous analysis. Fig. 2 shows the DTA-TGA of the sample underwent through several stages of decomposition when heated. The endothermic peak centered at 130 °C is assigned to the evaporation of absorbed water molecules. Major mass loss of the precursor occurred below 500 °C, corresponding to about 75 % of the total weight loss (43.3 %). The weight loss at lower temperatures is mainly due to the release of hydroxyl and partial carbonate. On the contrary, the weight loss at higher temperatures, almost completed around 1000 °C, is mainly caused by the further decomposition of carbonate species into oxide. The exothermic peak at 917 °C is attributed to the crystallization of YAG. This finding further supports the XRD results in Fig. 1 (a). In the XRD, the crystallization of the sample starts around 900 °C. This crystallization temperature is lower than the detected temperature by DTA. This is because of the exothermic peak in the DTA often lags behind crystallization as a result of the hysteresis of temperature [3].

3.3. Optical characterizations

3.3.1. Fourier transform infrared spectroscopy (FTIR)

Fig. 3 shows the FTIR spectra of the $Sm_{0.06}Y_{2.94}Al_5O_{12}$ as-prepared and calcined at 800 °C, 900 °C, and 1000 °C for 2 h. The spectra

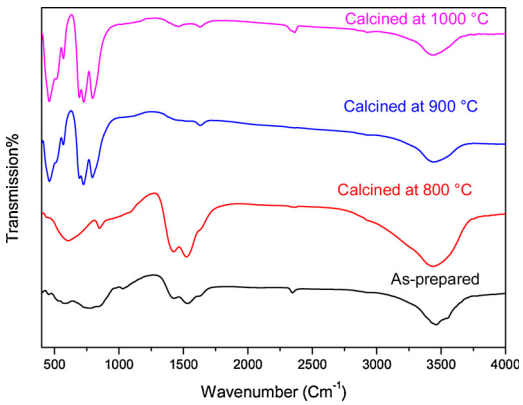

Fig. 3. FTIR spectra of $Sm_{0.06}Y_{2.94}Al_5O_{12}$ as-prepared and calcined at 800 °C, 900 °C and 1000 °C/2 h.

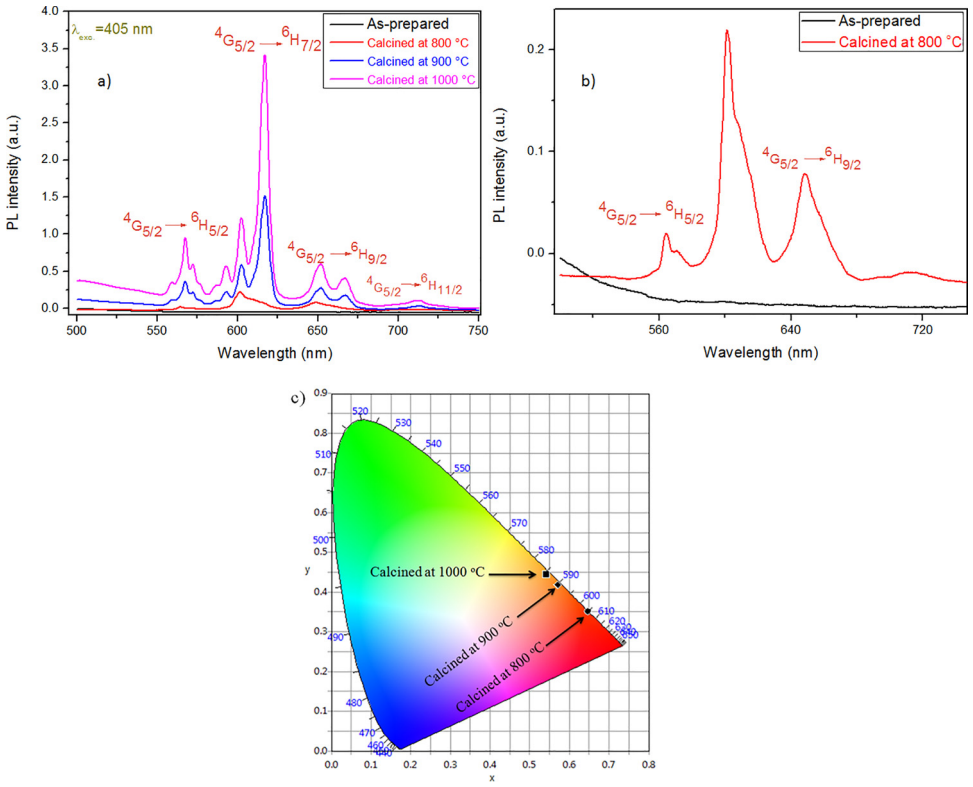

Fig. 4. (a) PL spectra of samples Sm $_{0.06}$ $Y_{2.94}Al_5O_{12}$ as-prepared and calcined at 800 °C, 900 °C and 1000 °C. (b) Zoom in on the PL spectra of samples as-prepared and calcined at 800 °C. (c) CIE chromaticity diagram of samples calcined at 800 °C, 900 °C and 1000 °C.

clearly show a broad absorption around 3418 cm^{-1} that can be assigned to the stretching vibration due to waterand yttrium/aluminum hydroxyl groups. Other peaks at 1522, 1426 and 854 cm^{-1} correspond to NH_4^+, CO_3^{2-} and HCO_3^{-1} ions in the bond-stretching mode, respectively. As calcination temperature increases, all the above peaks become weaker because of the decomposition of the precursor. In addition, in the case of calcination at 900 °C or above, new intense peaks in the range of $800-450$ cm^{-1} are appeared. These peaks represent the characteristic metal-oxygen vibration of YAG structure [17,18]. It is also noticed that these characteristics bands agree well with bands observed in YAG single crystal reported in [18].

3.3.2. Photoluminescence

Luminescence properties of phosphors are strongly influenced by its structural properties; such as particle size [19], surface morphology [20], and crystallinity [21]. Crystallinity is one of the most important parameter that plays a strong role in the luminescence behavior. Thus, the PL spectra of Sm $_{0.06}Y_{2.94}Al_5O_{12}$ nanopowders have been measured. Fig. 4 shows the measured PL spectra of as-prepared and calcined nanopowders at 800 °C, 900 °C, and 1000 °C excited by wavelength 405 nm. The maximum PL intensity was obtained from sample calcined at 1000 °C, while the as-prepared sample exhibits absence of the PL signal. In addition, the fundamental intense PL peak is located at 618 nm for samples calcined at 900 °C and 1000 °C, whereas it is located at 602 nm in the case of 800 °C. Moreover, the spectral shape of samples calcined at 900 °C and 1000 °C exhibits more splitted lines rather than the one calcined at 800 °C. In as-prepared sample, the absence of the PL related to Sm^{3+} ions points to the strong effect of the heat treatment on the optical activation of the emitting ions. Similar behavior has been reported in [22]. Enhancement of the PL intensity with increasing the calcined temperature can be linked to the improvement of the crystal structure with temperature, consistent with XRD results Fig. 1 (a). For instant, Murayama, M.et al. [22] explained the enhancement of the PL intensity from Sm ions due to the change in the local symmetry (coordination numbers and distances) around it.

These findings also in line with the results reported by Pan et al. [23]. The authors found that the emission intensity of cerium increases with increasing the annealing temperature and referred this to improvement of the crystallinity of YAG particles. This also supports by the drastic change in the PL features at temperature 900 °C compared to 800 °C.

At high calcined temperatures, 900 °C and1000 °C, the crystalline phase of YAG is formed and led to adjust the suitable local environment around Sm^{3+} ions which is adapted for better excitation and emission pathways. In addition, the fine analysis of the PL spectra of Sm ions embedded in a solid matrix can be used to determine the degree of symmetry in its local environment. The intensity ratio of electric dipole (ED) to magnetic dipole (MD) transitions has been used to measure the symmetry of the local environment of the trivalent 4*f* ions. It is well known that the magnetic dipole (MD) allowed transition obeys the selection rule $\Delta J = 0, \pm 1$. Hence, the transition $^4G_{5/2} \rightarrow {}^6H_{5/2}$, which follows the first condition ($\Delta J = 0$) is a MD in its nature. The transition $^4G_{5/2} \rightarrow$

$^6H_{7/2}$ with $\Delta J = \pm 1$ is a magnetic dipole (MD) allowed, but it is an electric dipole (ED) dominated. The other transition $^4G_{5/2} \rightarrow {}^6H_{9/2}$ is purely an electric dipole transition. Higher the intensity of the ED transition, more the asymmetry nature of the local environment around the ion [24,25]. Therefore, in our case, the emission spectrum of sample calcined at 800 °C, Fig. 4 (b), shows that the $^4G_{5/2} \rightarrow {}^6H_{9/2}$ (ED) transition is more intense than $^4G_{5/2} \rightarrow {}^6H_{5/2}$ (MD). This indicates the asymmetric nature of the local medium surrounding Sm ions. In contrast, as appeared in samples calcined at 900 °C and 1000 °C, the $^4G_{5/2} \rightarrow {}^6H_{5/2}$ (MD) transition exhibits higher intensity than $^4G_{5/2} \rightarrow {}^6H_{9/2}$ (ED), which indicates the symmetry environment around Sm ions due to the higher crystallinity at these calcined temperatures. Moreover, the spectral splitting in the PL can be attributed to the crystal field effect. Embedding Sm^{3+} in crystalline environment results in affecting its energy levels by the local field induced by the crystal. Such effect is known as Stark effect. This is the reason why sample calcined at 800 °C, amorphous-like, shows a non-splitting PL spectrum with broad bands. Unlike the crystalline samples calcined at 900 °C and1000 °C. It is worth to mention that similar PL spectrum of sample calcined at 800 °C have been reported from Sm-doped glass i.e. amorphous matrices [26,27]. This rather supports our interpretation. Hence, it can be concluded that the PL spectral features of the Sm ions can be influenced by the annealing/calcined temperature and/or time. In addition, this effect is linked to the (local) crystal structure of the sample. On the other hand, from the emission color point of view, CIE chromaticity diagram is used to examine the emission color and the color purity at each calcined temperature. It can be observed that all samples are located in the reddish-orange region with calculated coordinates (0.6478, 0.3518), (0.5708, 0.4182), and (0.5412, 0.444) for calcined temperature 800 °C, 900 °C, and 1000 °C, respectively. This fine tunability of the emission color further indicates the significance of the calcined temperature on manipulating the final color purity. This is of great importance in terms of white light emitting applications.

For gaining more information about the excitation levels of Sm in the crystalline material, PLE has been measured. PLE is a powerful technique to probe the excitation levels of specific emission line. By monitoring the intense emission wavelength at 618 nm, $^4G_{5/2} \rightarrow {}^6H_{7/2}$, transition in $Sm_{0.06}Y_{2.94}Al_5O_{12}$ nanocrystals, the UV-Visible PLE spectrum is obtained, as shown in Fig. 5. It is found that the PLE spectrum is composed of nine excitation bands originated from 4*f*-4*f* inner shell transition within the ($4f^5$) configuration of the Sm^{3+} ions. The dominant bands are found at around 309 nm, 407 nm and 467 nm. The assignments of these bands are given in Table 1. Similar results have been reported in Sm^{3+}-doped different hosts [28,29] with slight differences in the peaks position due to the different crystal field strength of each host materials.

It is worth to mention that the measured excitation wavelengths cover the region from UV to bluish–green, which point to the match of these wavelenthes with the commercial UV/blue laser diodes, blue and bluish – green LED's and Ar^+ laser that can be used as powerful pumping sources for Sm-doped YAG in the present work. These can be verified by measuring the PL spectra of $Sm_{0.06}Y_{2.94}Al_5O_{12}$ sample excited by some available wavelengths in our laboratory (405,455, 488, and 532 nm). Fig. 6 shows the PL spectra under different excitation wavelengths. It is found that, all of these spectra reveal the same emission transitions; $^4G_{5/2} \rightarrow {}^6H_{5/2}$ (567 nm), $^4G_{5/2} \rightarrow {}^6H_{7/2}$ (618 nm), $^4G_{5/2} \rightarrow {}^6H_{9/2}$ (652 nm), and $^4G_{5/2} \rightarrow {}^6H_{11/2}$ (712 nm). In addition, the excitation by 405 nm reveals the highest PL intensity in compared to the other excitation wavelengths, agrees with the PLE in Fig. 5. Furthermore, there is no observable shift in the PL peak positions due to change the excitation wavelength. This likely indicates that the emitting state is the same whatever the excitation wavelength.

4. Conclusion

Sm-doped YAG, $Sm_{0.06}Y_{2.94}Al_5O_{12}$, nanocrystals have been synthesized by reverse strike co-precipitation method. It is found that the crystallization temperature of the prepared powders was around 900 °C, as measured by DTA. The crystalline phase, at this calcination temperature, has been also confirmed by XRD results. In addition, higher calcination temperature, 1000 °C, was favorable to improve the crystallinity of the nanopowders. The XRD has also evidenced the transformation from amorphous phase, in as-prepared, to the onset of the crystallization, at 800 °C, to crystalline phase, at 900 °C. Moreover, a correlation between the

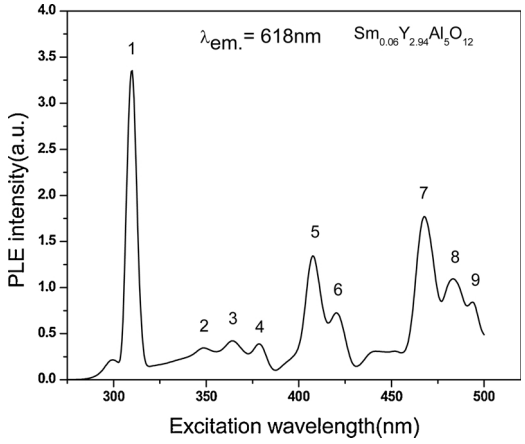

Fig. 5. PLE spectrum of $Sm_{0.06}Y_{2.94}Al_5O_{12}$ calcined at 1000 °C monitored at 618 nm emission peak.

Table 1
The assignments of the PLE peak of $Sm_{0.06}Y_{2.94}Al_5O_{12}$ calcined at 1000 °C monitored at 618 nm emission line.

Transition No.	Transition assignment	Wavelength (nm)
1	$^3H_{5/2} \rightarrow {}^3H_{9/2}$	309
2	$^3H_{5/2} \rightarrow {}^3H_{7/2}$	347
3	$^3H_{5/2} \rightarrow {}^4F_{9/2}$	363
4	$^3H_{5/2} \rightarrow {}^4D_{5/2}$	378
5	$^3H_{5/2} \rightarrow {}^4K_{11/2}$	407
6	$^3H_{5/2} \rightarrow {}^6P_{5/2} + M_{19/2}$	420
7	$^3H_{5/2} \rightarrow {}^4F_{5/2} + {}^4I_{13/2}$	467
8	$^3H_{5/2} \rightarrow {}^4F_{5/2} + {}^4I_{13/2}$	482
9	$^3H_{5/2} \rightarrow {}^4G_{7/2} + {}^4I_{11/2} + {}^4M_{15/2}$	494

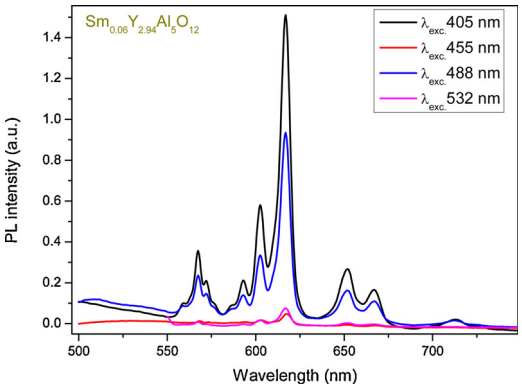

Fig. 6. PL spectra of $Sm_{0.06}Y_{2.94}Al_5O_{12}$, calcined at 1000 °C, excited by different excitation wavelengths.

photoluminescence response, of the amorphous phase and crystalline phase, with the XRD findings has been established. The PL spectral modifications in the Sm-doped crystalline YAG were attributed to the crystal field effect of the local crystalline environment. Furthermore, the relative intensity between the emission lines inferred the local symmetry around Sm ions. The CIE chromaticity diagram has also showed the influence of calcined temperature on the reddish-orange color tunability. These results highlight on the advantage of the PL, as efficient and nondestructive tool, to reflect inherent feature such as the local crystalline property of the material. This can be used as a guideline for testing the prepared nanocrystals before the further processing to fabricate the end ceramic product.

Declaration of Competing Interest

The authors declare that they have no known competing financialinterestsor personal relationships that could have appeared to influence the work reported in this paper.

References

[1] M. Nazarov, D.Y. Noh, New Generation of Europium- and Terbium-Activated Phosphors: From Syntheses to Applications, Pan Stanford, 2011.
[2] M.L. Saladino, E. Caponetti, Opt. Mater. 32 (2009) 89–93.
[3] C. Marlot, E. Barraud, S. Le Gallet, M. Eichhorn, F. Bernard, J. Solid State Chem. 191 (2012) 114–120.
[4] C.-H. Lu, H.-C. Hong, R. Jagannathan, J. Mater. Chem. 12 (2002) 2525–2530.
[5] L. Zhang, Z. Lu, J. Zhu, H. Yang, P. Han, Y. Chen, Q. Zhang, J. Rare Earth. 30 (2012) 289–296.
[6] M. Xu, Z. Zhang, J. Zhao, J. Zhang, Z. Liu, J. Alloys Compd. 647 (2015) 1075–1080.
[7] J.-G. Li, T. Ikegami, J.-H. Lee, T. Mori, Y. Yajima, J. Eur. Ceram. Soc. 20 (2000) 2395–2405.
[8] L. Wang, H. Kou, Y. Zeng, J. Li, Y. Pan, X. Sun, J. Guo, Ceram. Int. 38 (2012) 3763–3771.
[9] J.-G. Song, F. Wang, M.-H. Xu, Y.-Y. Ju, Y.-L. Li, S.-B. Li, G.-C. Ji, J. Ceram. Process Res. 13 (2012) 154–157.
[10] P. Apte, H. Burke, H. Pickup, J. Mater. Res. 7 (1992) 706–711.
[11] J. Li, F. Chen, W. Liu, W. Zhang, L. Wang, X. Ba, Y. Zhu, Y. Pan, J. Guo, J. Eur. Ceram. Soc. 32 (2012) 2971–2979.
[12] J.-G. Li, T. Ikegami, J.-H. Lee, T. Mori, J. Mater. Res. 15 (2000) 1514–1523.
[13] A. Verma, M. Nath, N. Malhan, A.K. Ganguli, Mater. Lett. 93 (2013) 21–24.
[14] B. Ma, T. Lu, N. Wei, Z. Lu, F. Li, X. Chen, Y. Guan, W. Zhang, Int. J. Appl. Ceram. Tec. 12 (2015) 1230–1238.
[15] P. Palmero, R. Traverso, Materials (Basel, Switzerland) 7 (2014) 7145–7156.
[16] A. Ikesue, T. Kinoshita, K. Kamata, K. Yoshida, J. Am. Ceram. Soc. 78 (1995) 1033–1040.
[17] H. Gong, D.-Y. Tang, H. Huang, J. Ma, J. Am. Ceram. Soc. 92 (2009) 812–817.
[18] X.-X. Ge, Y.-H. Sun, C. Liu, W.-K. Qi, J. Sol-Gel Sci. Technol. 52 (2009) 179–187.
[19] W.-N. Wang, W. Widiyastuti, T. Ogi, I.W. Lenggoro, K. Okuyama, Chem. Mater. 19 (2007) 1723–1730.
[20] X. He, X. Liu, R. Li, B. Yang, K. Yu, M. Zeng, R. Yu, Sci. Rep. 6 (2016) 22238.

[21] W.-H. Chao, R.-J. Wu, T.-B. Wu, J. Alloys Compd. 506 (2010) 98–102.
[22] M. Murayama, K. Yoda, K. Shiraishi, S. Guan, S. Komuro, X. Zhao, OPJ 08 (2018) 19.
[23] Y. Pan, M. Wu, Q. Su, Mater. Sci. Eng. B 106 (2004) 251–256.
[24] M. Kumar, V. Natarajan, S.V. Godbole, Bull. Mater. Sci. 37 (2014) 1205–1214.
[25] S. Selvi, K. Marimuthu, G. Muralidharan, J. Lumin. 159 (2015) 207–218.
[26] V. Thomas, R.G.S. Sofin, M. Allen, H. Thomas, P.R. Biju, G. Jose, N.V. Unnikrishnan, Spectrochim. Acta A 171 (2017) 144–148.
[27] M. Elisa, B.A. Sava, I.C. Vasiliu, R.C.C. Monteiro, J.P. Veiga, L. Ghervase, I. Feraru, R. Iordanescu, J. Non-Cryst. Solids 369 (2013) 55–60.
[28] L. Van Vu, D.T.M. Huong, V.T.H. Yen, N.N. Long, Mater. Trans. 56 (2015) 1422–1424.
[29] H.M. Ha, T.T.Q. Hoa, L. Van Vu, N.N. Long, J. Mater, Sci.: Mater. Electron. 28 (2017) 884–891.